A Hybrid Current-Power Optimal Power Flow Technique

Whei-Min Lin, *Member, IEEE*, Cong-Hui Huang, and Tung-Sheng Zhan

Abstract—**An equivalent current injection (ECI)-based hybrid current-power optimal power flow (OPF) model is proposed in this paper, and the predictor-corrector interior point algorithm (PCIPA) is tailored to fit the OPF for solving nonlinear programming (NLP) problems. The proposed method can further decompose into two subproblems. The computational results of IEEE 9 to 300 buses have shown that the proposed algorithms can enhance the performance in terms of the number of iterations, memory storages, and CPU times.**

Index Terms—**Equivalent current injection, nonlinear programming, optimal power flow, predictor-corrector interior point algorithm.**

I. Introduction

OPTIMAL power flow was first discussed [1] in 1962 and took a long time to become a successful algorithm that could be applied for everyday uses [2], [3]. OPF can be applied not only in the system planning but also in the real-time operation for power systems in the deregulation environment. Reference [4] provided an overall introduction on the lambda-iteration method, gradient method, Newton's method, and the linear programming (LP) technique for solving OPF problems.

With Karmarkar's publication [5] in 1984, many interior point algorithms (IPAs) for the linear programming and quadratic programming (QP) have been proposed. In recent years, the primal-dual interior point algorithm (PDIPA) has been extensively applied to solve problems such as the OPF [6], [7], state estimation [8], security constrained OPF [9], and optimal reactive power flow [10]. Numerical results show that PDIPA has a great potential for solving problems of power systems operation and planning, as compared with many conventional methods, including the Newton's method [11].

In 1992, Mehrotra proposed best-search directions that defined the predictor and corrector steps which then generated the PCIPA [12]. The use of the PCIPA may improve the convergent performance, resulting in a small number of iterations.

A current injection algorithm based on the use of a constant nodal admittance matrix was described in [13], which discussed, in a tutorial nature, that this algorithm cannot be used for general power flow (PF) applications because a satisfactory method of modeling generator PV nodes with currents has not yet been developed, which could cause convergent instability or even divergence.

Experiencing these PV difficulties in publishing [14], [15] by the author(s), current based power flow of [14] was developed for distribution networks *only*, where generator PV buses are not common and can be omitted. We can get a constant Jacobian matrix which needs to be factorized only once. Reference [15] successfully implements the current power flow for high voltage networks, with a new idea of resolving the PV bus by using a single active power mismatch equation and an associated voltage deviation instead of the intuitive current conversion which could cause divergence. We can get a nearly constant Jacobi with a few generator buses still state-dependent and need to be updated at each iteration.

Pioneering the rectangular-form current-based OPF, [16] did a brief test with rectangular nodal voltages and branch currents used for state variables. The generator PV problem was avoided by replacing the PV bus with real and reactive power (PQ) directly; however, the oversimplification by replacing PV with PQ is not a common practice in handling generator buses. Besides, using KCL in [16], it was not even mentioned how load and generator power injections are handled for each iteration, which are the key factors affecting convergent behaviors in developing a current-based model. Reference [17] developed a rectangular voltage OPF, but the power flow equations are still PQ based, not current.

The constrained nonlinear optimization problem in this paper is solved using PCIPA that permits the efficient and effective handling of large sets of equality (power flow) and inequality (limits) constraints. The OPF uses rectangular form for both the voltage and current, and current mismatch equations are used for power flow calculation with the PV buses specifically treated by the model of [15] to ensure the numerical stability. The OPF problem can also be decoupled into two small subproblems [18] to further enhance the performance. Optimization can be accomplished by repeatedly solving the two subproblems.

II. Notation

The following symbols are used throughout this paper. Some symbols are also defined in the text where they first appear.

Symbols

$\Delta(\cdot)$	Change in variables.
$\nabla(\cdot)$	Differentiation operation.

Manuscript received November 29, 2006; revised August 30, 2007. Paper no. TPWRS-00831-2006.

W.-M. Lin and C.-H. Huang are with the Department of Electrical Engineering, National Sun Yat-Sen University, Kaohsiung 80424, Taiwan, R.O.C. (e-mail: wmlin@ee.nsysu.edu.tw).

T.-S. Zhan is with the Department of Electrical Engineering, Kao-Yuan University, Lu-Chu Hsiang, Kaohsiung 821, Taiwan, R.O.C. (e-mail: tszhan@cc.kyu.edu.tw).

Digital Object Identifier 10.1109/TPWRS.2007.913301

$\underline{(\cdot)}, \overline{(\cdot)}$	Subscripts denoting lower and upper limit.
$(\cdot)^T$	Superscript denoting transpose.
$(\cdot)^{spec}$	Specified constant.
$(\cdot)^{cal}$	Calculated value of each iteration.
P	Active power.
Q	Reactive power.

Vectors

$\underline{\omega}$	Lower limit slack variables for inequality constraints.
$\overline{\omega}$	Upper limit slack variables for inequality constraints.
$\underline{z}$	Lower limit dual variables for inequality constraints.
$\overline{z}$	Upper limit dual variables for inequality constraints.
$\underline{h}$	Inequality constraints lower limit.
$\overline{h}$	Inequality constraints upper limit.
λ	Lagrangian multiplier for power flows.
x	Problem variables for minimum cost.
$\tilde{e}$	Column vector of ones.

Matrices

Y_G	Real component of Y (admittance) matrix.
Y_B	Imaginary component of Y matrix.
H	Augmented Hessian matrix.
$\underline{W}$	Diagonal matrix: $diag(\underline{\omega}_j)$.
$\overline{W}$	Diagonal matrix: $diag(\overline{\omega}_j)$.
$\underline{Z}$	Diagonal matrix: $diag(\underline{z}_j)$.
$\overline{Z}$	Diagonal matrix: $diag(\overline{z}_j)$.

III. Equivalent Current Injection Model

The complex bus voltages are defined in Cartesian form as

$$V_i = e_i + jf_i \tag{1}$$

where e_i and f_i are, respectively, the real and imaginary components of V_i.

A. Equations for PQ Buses

From the transmission line π model in Fig. 1, the rectangular form current injections are

$$\begin{aligned} I_i &= \{g_{ij}(e_i - e_j) - b_{ij}(f_i - f_j) - b_c f_i\} \\ &\quad + j\{g_{ij}(f_i - f_j) + b_{ij}(e_i - e_j) + b_c e_i\} \qquad (2) \\ I_j &= \{g_{ij}(e_j - e_i) - b_{ij}(f_j - f_i) - b_c f_j\} \\ &\quad + j\{b_{ij}(e_j - e_i) + g_{ij}(f_j - f_i) + b_c e_j\} \qquad (3) \end{aligned}$$

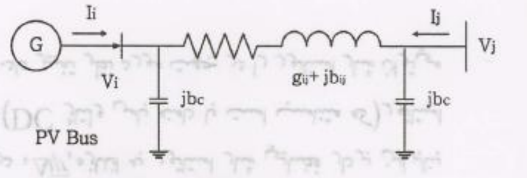

Fig. 1. Transmission line equivalent π model.

where $I_i = I_{i,r} + I_{i,i}$ and $I_j = I_{j,r} + I_{j,i}$.

From above, the Newton–Raphson algorithm can be written in the ECI form [14] at the kth iteration by considering all PQ buses, that is

$$\left[\begin{array}{c} \Delta I_{i,r}^k \\ \hline \Delta I_{i,i}^k \end{array}\right] = \left[\begin{array}{c|c} Y_G & -Y_B \\ \hline Y_B & Y_G \end{array}\right] \left[\begin{array}{c} \Delta e_i^k \\ \hline \Delta f_i^k \end{array}\right] \tag{4}$$

where the current mismatches are defined by the specified value (spec) minus the calculated (cal) value as

$$\begin{aligned} \Delta I_{i,r} &= \Delta I_{i,r}^{spec} - \Delta I_{i,r}^{cal} \\ \Delta I_{i,i} &= \Delta I_{i,i}^{spec} - \Delta I_{i,i}^{cal} \end{aligned} \tag{5}$$

and

$$\begin{aligned} e^{k+1} &= e^k + \Delta e^k \\ f^{k+1} &= f^k + \Delta f^k. \end{aligned} \tag{6}$$

The specified constant power load P^{spec} and Q^{spec} can be converted into the specified ECI current load [14] with the calculated voltage for bus i at the kth iteration by

$$I_i^{spec} = \frac{(P_i - jQ_i)^{spec}}{(V_i^k)^*} = I_{i,r}^{spec} + jI_{i,i}^{spec}. \tag{7}$$

B. Representation of PV Buses

For a PV bus, its injected real power and voltage are given by

$$P_i = \mathrm{Re}\,[V_i \times I_i^*] = e_i \cdot I_{i,r} + f_i \cdot I_{i,i} \tag{8}$$

$$|V_i|^2 = e_i^2 + f_i^2. \tag{9}$$

Using Taylor's expansion of (8) and (9) [15] to substitute for ΔI in (4), it can get

$$\left[\begin{array}{c} \Delta P_i \\ \hline \Delta|V_i|^2 \end{array}\right] = \left[\begin{array}{c|c} J_1 & -J_2 \\ \hline J_3 & J_4 \end{array}\right] \left[\begin{array}{c} \Delta e_i \\ \Delta e_j \\ \hline \Delta f_i \\ \Delta f_j \end{array}\right]$$

$$\begin{aligned} J_1 &= \left[(e_i \cdot g_{ij} + f_i \cdot b'_{ij} + I_{i,r})\ (-e_i \cdot g_{ij} - f_i \cdot b_{ij})\right] \\ J_2 &= \left[(-e_i \cdot b'_{ij} + f_i \cdot g_{ij} + I_{i,i})\ (e_i \cdot b_{ij} - f_i \cdot g_{ij})\right] \end{aligned}$$

$$
\begin{aligned}
J_3 &= [2e_i 0] \\
J_4 &= [2f_i 0]
\end{aligned} \tag{10}
$$

where

$$
\begin{aligned}
\Delta P_i &= P_i^{spec} - P_i^{cal} \\
\Delta |V_i|^2 &= |V_i^{spec}|^2 - |V_i^{cal}|^2
\end{aligned}
$$

with $b'_{ij} = b_{ij} + b_c$. This implementation maintains the 2n × 2n Jacobian matrix structure with a pair of variables ΔP_i and $\Delta |V_i|^2$ for each PV bus.

IV. OPF Problem With PCIPA

A general version of the problem can be shown as

$$
\begin{aligned}
&minimizing\ f(x) \\
&s.t. \\
&\qquad g(x) = 0 \\
&\qquad \underline{h} \le h(x) \le \overline{h}.
\end{aligned} \tag{11}
$$

Transform all inequality constraints in the NLP problem (11) into equalities by adding positive slack vectors $\omega_j \ge 0$ as

$$
\begin{aligned}
&Min \quad f(x) \\
&s.t. \\
&\qquad g(x) = 0 \\
&h(x) - \underline{\omega} - \underline{h} = 0 \\
&h(x) + \overline{\omega} - \overline{h} = 0 \\
&\qquad (\underline{\omega}, \overline{\omega}) \ge 0.
\end{aligned} \tag{12}
$$

A full-scale OPF considers all available controls, such as the generator power, load, phase shifters and reactors for P control, and the generator voltage, capacitor banks, and transformer taps for Q control. For illustrative purposes, although a complete power flow program of [14], [15] was used in this study, only P and V are used for control variables, i.e., the generator dispatchable active power (P_G) is used for P control, and the voltage magnitude ($|V_G|$) is used for Q control. The state variables are rectangular voltages with real and imaginary parts (e, f). Limits of the associated control variables P and V are considered for inequality constraints together with line limits of apparent power. Again, as a common example, the objective function to minimize the generator fuel cost is used. An OPF problem with PCIPA of (11) may be formulated as

$$
Min \quad f(x) = \sum_{i=1}^{NG} a_i P_{Gi}^2 + b_i P_{Gi} + c_i \tag{13}
$$

subject to

1) $g(x)$ by

$$
\begin{cases}
\left.\begin{array}{l} -\mathrm{I_r^{spec}} + \mathrm{I_r^{cal}} = 0 \\ -\mathrm{I_i^{spec}} + \mathrm{I_i^{cal}} = 0 \end{array}\right\} \Rightarrow pq \quad bus \\
\left.\begin{array}{l} -\mathrm{P_G} + \mathrm{P_{Load}} + \mathrm{P^{cal}} = 0 \\ \quad -|\mathrm{V_G}|^2 + |\mathrm{V^{cal}}|^2 = 0 \end{array}\right\} \Rightarrow pv \quad bus
\end{cases} \tag{14}
$$

where power balance constraints are given in (4) and (10).

2) $h(x)$ by

$$
\begin{cases}
\mathrm{S_{ij}^2} \le \overline{\mathrm{S}}_{L,ij}^2 \\
S_{\mathrm{ji}}^2 \le \overline{\mathrm{S}}_{L,ij}^2 \\
\underline{\mathrm{P_{Gi}}} \le \mathrm{P_{Gi}} \le \overline{\mathrm{P_{Gi}}} \\
|\underline{\mathrm{V_i}}|^2 \le (\mathrm{e_i^2} + f_i^2) \le |\overline{\mathrm{V_i}}|^2
\end{cases} \tag{15}
$$

where

a_i, b_i, c_i	fuel cost coefficients of thermal plant i;
$\lvert V_i \rvert$	voltage magnitude at bus i;
e_i, f_i	real and imaginary part of voltage V_i at bus i;
P_{Gi}	dispatchable active power at bus i;
(i, j)	transmission line connecting buses i and j;
S_{ij}^2, S_{ji}^2	apparent power of transmission line (i, j) or (j, i);
$\overline{S}_{L,ij}^2, \overline{S}_{L,ji}^2$	apparent power limit of transmission line (i, j) or (j, i), where $\overline{S}_{L,ij}^2 = \overline{S}_{L,ji}^2$.

As a more general problem, other control variables or objective functions can be added or used similarly as stated above, together with related limits, which will affect the size and variables involved in forming the Hessian, but the solving procedure will be the same.

Using slack variables ω to transform inequality constraints into equality constraints and adding barrier penalties to the original objective function, the Lagrangian is given by

$$
\begin{aligned}
\mathcal{L} = &\sum_{i}^{NG} \left(a_i P_{Gi}^2 + b_i P_{Gi} + c_i\right) \\
&- \lambda^T \begin{bmatrix} I_r^{cal} - I_r^{spec} \\ I_i^{cal} - I_i^{spec} \\ P_G^{cal} - P_G^{spec} - P_{load} \\ |V_G^{cal}|^2 - |V_G^{spec}|^2 \end{bmatrix} - \underline{Z_G^T}(P_G - \underline{\omega_G} - \underline{P_G}) \\
&+ \overline{Z_G^T}(P_G + \overline{\omega_G} - \overline{P_G}) - \underline{Z_v^T}\left(|V|^2 - \underline{\omega_v} - |\underline{V}|^2\right) \\
&+ \overline{Z_v^T}\left(|V|^2 - \overline{\omega_v} - |\overline{V}|^2\right) + \overline{Z_{S,ij}^T}\left(S_{ij}^2 + \overline{\omega_{S,ij}} - \overline{S_L^2}\right) \\
&+ \overline{Z_{S,ji}^T}\left(S_{ji}^2 + \overline{\omega_{S,ji}} - \overline{S_L^2}\right) \\
&- \mu \sum_{i=1}^{N} \ln(\underline{\omega_G} + \overline{\omega_G} + \underline{\omega_v} + \overline{\omega_v} + \overline{\omega_{S,ij}} + \overline{\omega_{S,ji}})
\end{aligned} \tag{16}
$$

where $\mu^k > 0$ is the IPA barrier parameter that monotonically decreases to zero as iterations progress. Based on the KKT optimality condition, a set of nonlinear equations can be derived from (16), and the corresponding set of linear correction equations can be derived in sequence by applying the Newton's method [7], [17], [19]. According to the KKT, the Hessian matrix is obtained as

$$\begin{bmatrix} \nabla_x^2\mathcal{L} & -J_g^T & -J_{\underline{h}}^T & J_{\overline{h}}^T & 0 & 0 \\ -J_g & 0 & 0 & 0 & 0 & 0 \\ -J_{\underline{h}} & 0 & 0 & 0 & I & 0 \\ J_{\overline{h}} & 0 & 0 & 0 & 0 & I \\ 0 & 0 & \underline{W} & 0 & \underline{Z} & 0 \\ 0 & 0 & 0 & \overline{W} & 0 & \overline{Z} \end{bmatrix} \times \begin{bmatrix} \Delta x \\ \Delta\lambda \\ \Delta\underline{z} \\ \Delta\overline{z} \\ \Delta\underline{\omega} \\ \Delta\overline{\omega} \end{bmatrix} = - \begin{bmatrix} \nabla_x\mathcal{L} \\ \nabla_\lambda\mathcal{L} \\ \nabla_{\underline{z}}\mathcal{L} \\ \nabla_{\overline{z}}\mathcal{L} \\ \nabla_{\underline{\omega}}\mathcal{L} \\ \nabla_{\overline{\omega}}\mathcal{L} \end{bmatrix} \tag{17}$$

where $J_g = \nabla_x(x)$, $J_h = \nabla_x h(x)$, and $\nabla_x^2\mathcal{L}$ shows as

$$\nabla_x^2\mathcal{L} = H_f(x^k) - \sum_{j=1}^{m} \lambda_j^k H_{gj}(x^k) + \sum_{j=1}^{p} \left(\overline{z}_j^k - \underline{z}_j^k\right) H_{hj}(x^k). \tag{18}$$

The upper left block of (17) is an augmented Hessian matrix. The elements of Hessian matrix are the second-order partial derivatives of the augmented objective function with respect to all variables.

For iteration k, the Newton direction can be obtained by first solving the reduced system [19]

$$\begin{bmatrix} J_r & -J_g^T \\ -J_g & 0 \end{bmatrix} \begin{bmatrix} \Delta x \\ \Delta\lambda \end{bmatrix} = - \begin{bmatrix} \nabla_x\mathcal{L} \\ \nabla_\lambda\mathcal{L} \end{bmatrix} \tag{19}$$

where

$$J_r = \nabla_x^2\mathcal{L} + \mu^k \left(J_{\underline{h}}^T \underline{W}^{-2} J_{\underline{h}} + J_{\overline{h}}^T \overline{W}^{-2} J_{\overline{h}} \right) \tag{20}$$

and then compute

$$\begin{aligned} \Delta\underline{\omega} &= J_{\underline{h}} \Delta x \\ \Delta\overline{\omega} &= -J_{\overline{h}} \Delta x \\ \Delta\underline{z} &= -\mu^k \underline{W}^{-2} \Delta\underline{\omega} \\ \Delta\overline{z} &= -\mu^k \overline{W}^{-2} \Delta\overline{\omega}. \end{aligned} \tag{21}$$

After solving (19) and (21) for the adjustment terms at iteration k, the barrier parameter μ^k was dynamically estimated by

$$\mu = \tau \times \left(\frac{gap^*}{gap}\right)^2 \times \left(\frac{gap^*}{2 \times (nv + nc)}\right) \tag{22}$$

where τ is the centering parameter with $\tau \in (0,1)$; nv and nc are the numbers of variables and constraints, respectively. gap^* is the complementary gap considering variable updates; and gap is also a complementary gap without considering variable updates [19]. We have

$$gap = \underline{\omega} \times \underline{z} + \overline{\omega} \times \overline{z} \tag{23}$$

and

$$\begin{aligned} gap^* = {} & (\underline{\omega} + \alpha_p \times \Delta\underline{\omega}) \times (\underline{z} + \alpha_d \times \Delta\underline{z}) \\ & + (\overline{\omega} + \alpha_p \times \Delta\overline{\omega}) \times (\overline{z} + \alpha_p \times \Delta\overline{z}) \end{aligned} \tag{24}$$

where α_p and α_d are the step sizes of primal and the dual variables, respectively. They are chosen as

$$\begin{aligned} \alpha_p = \min \Bigg\{ \sigma \times \min \Bigg[-\frac{\underline{\omega}_j}{\Delta\underline{\omega}_j}, -\frac{\overline{\omega}_j}{\Delta\overline{\omega}_j}, \\ if(\Delta\underline{\omega}_j < 0, \Delta\overline{\omega}_j < 0) \Bigg], 1 \Bigg\} \end{aligned} \tag{25}$$

$$\begin{aligned} \alpha_d = \min \Bigg\{ \sigma \times \min \Bigg[-\frac{\underline{z}_j}{\Delta\underline{z}_j}, -\frac{\overline{z}_j}{\Delta\overline{z}_j}, \\ if(\Delta\underline{z}_j < 0, \Delta\overline{z}_j < 0) \Bigg], 1 \Bigg\} \end{aligned} \tag{26}$$

where σ is a safety factor chosen to be less than 1, and 0.99995 works well for the total generation cost problem. In some IPA nonlinear programming problems, only one step length is used. For the minimum total generation cost problem, the use of different step lengths for primal and dual variables resulted in a better performance [19].

In terms of the KKT first-order necessary condition of (16) and the Newton's method [19], (17) may get the correction equations as

$$[H] \times \begin{bmatrix} \Delta x \\ \Delta\lambda \\ \Delta\underline{z} \\ \Delta\overline{z} \\ \Delta\underline{\omega} \\ \Delta\overline{\omega} \end{bmatrix} = \begin{bmatrix} -\nabla_x\mathcal{L} \\ -\nabla_\lambda\mathcal{L} \\ -\nabla_{\underline{z}}\mathcal{L} \\ -\nabla_{\overline{z}}\mathcal{L} \\ \mu \cdot \tilde{e} - \underline{W} \cdot \underline{Z} \cdot \tilde{e} - \Delta\underline{W} \cdot \Delta\underline{Z} \cdot \tilde{e} \\ \mu \cdot \tilde{e} - \overline{W} \cdot \overline{Z} \cdot \tilde{e} - \Delta\overline{W} \cdot \Delta\overline{Z} \cdot \tilde{e} \end{bmatrix} \tag{27}$$

where H is the Hessian matrix of (17).

PCIPA differs from IPA by (27) which introduces second-order terms $\Delta\underline{W} \cdot \Delta\underline{Z} \cdot \tilde{e}$ and $\Delta\overline{W} \cdot \Delta\overline{Z} \cdot \tilde{e}$. These nonlinear terms of (27) can be solved by the predictor and corrector steps in [19]. The OPF algorithm can be summarized in the flowchart of the PCIPA in Fig. 2.

Numerical Advantage: Taylor series expansion of a quadratic function terminates at the second-order term with no truncation error, that is

$$\begin{aligned} f(x^k + \Delta x) &= f(x^k) + (x^k)^T A \Delta x + \frac{1}{2} \Delta x^T A \Delta x \\ &= f(x^k) + \nabla f(x^k)^T \Delta x + f(\Delta x). \end{aligned} \tag{28}$$

From (28), it can be seen that if the objective function and constraints can be modeled properly with linear or quadratic functions [16], [17], control and state variables can be avoided in forming the Hessian; otherwise, a general OPF problem

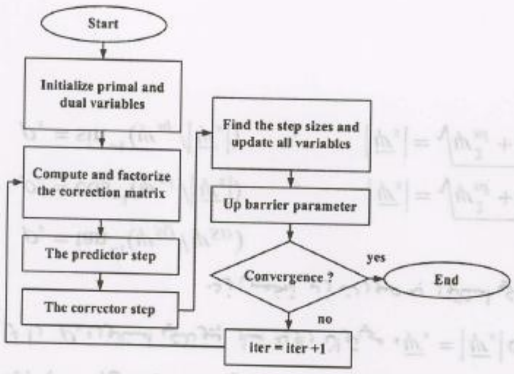

Fig. 2. Flowchart of the PCIPA.

could have these variables involved besides the Lagrangian multipliers.

Note that from (17) and the Jacobi in (4) and (10), the proposed method has a nearly constant Jacobi J_g, except for a few elements of the generator PV buses which need to be updated, while the traditional Newton–Raphson OPF has a state-dependent J_g, which needs to modify all elements at each iteration and is time-consuming. Besides, the proposed method has a decoupled version where J_g is constant without needing to update any element at all to gain more numerical advantages.

Decoupling: For PV buses, some assumptions can be made for simplification to further improve the performance [15].

1) From (10), $(g_{ij} \cdot e_i + b_{ij} \cdot f_i)^2 + (g_{ij} \cdot f_i + b_{ij} \cdot e_i)^2 \gg (I_{i,r}^2 + I_{i,i}^2)$, $I_{i,r}$ and $I_{i,i}$ are no more than one-tenth of the other components, and are negligible.
2) We have the general assumptions of
   - $|V_i| \cdot \cos\theta_i \gg |V_i| \cdot \sin\theta_i$
   - $|V_i| \cong 1.0$.
3) Network has low R/X ratio, that is, $R \ll X$ or $G \ll B$.

From (4) and (10), we can again get a constant matrix as shown in (29) at the bottom of the page.

That is, (40) decomposes into two submatrices as

$$J_g'' = \begin{bmatrix} -b_{11} & \cdots & -b_{1i} & \cdots & -b_{1n} \\ \vdots & \ddots & \vdots & \iddots & \vdots \\ -b_{i1} & \cdots & -b_{ii} & \cdots & -b_{in} \\ \vdots & \iddots & \vdots & \ddots & \vdots \\ -b_{n1} & \cdots & -b_{ni} & \cdots & -b_{nn} \end{bmatrix} \text{ and}$$

$$J_g''' = \begin{bmatrix} b_{11} & \cdots & b_{1i} & \cdots & b_{1n} \\ \vdots & \ddots & \vdots & \iddots & \vdots \\ 0 & \cdots & 2 & \cdots & 0 \\ \vdots & \iddots & \vdots & \ddots & \vdots \\ b_{n1} & \cdots & b_{ni} & \cdots & b_{nn} \end{bmatrix}$$

where J_g'' is the Jacobi of the decoupled active subproblem and J_g''' is Jacobi of the decoupled voltage subproblem with positions of the PV buses replaced by 0 and 2.

The reduced OPF problem can now be decomposed to two suboptimal problems as

1) active suboptimal problem with active variables (P_g, f) and associated constraints;
2) voltage suboptimal problem with voltage variable $(|V|^2, e)$ and associated constraints.

As stated above, the KKT condition from (16) can also be decomposed to two decoupled Hessian matrices [20]. The procedures of solving the decoupled version of IPA with the complementary duality gaps gap^a and gap^v for the active and voltage problems, respectively, are stated below [18].

Step 0: *Initialization.*

WHILE $(\mu^k = \varepsilon_\mu)$ DO:

Step 1) Run PCIPA to solve the active subproblem, and compute the associated complementary gap^a for active subproblem variables. If $gap^a/gap^v > \xi$, repeat solving this subproblem until $gap^a/gap^v \le \xi$; otherwise, go to step 2.

$$J_g' = \left[\begin{array}{ccccc|ccccc} 0 & \cdots & 0 & \cdots & 0 & -b_{11} & \cdots & -b_{1i} & \cdots & -b_{1n} \\ \vdots & \ddots & \vdots & \iddots & \vdots & \vdots & \ddots & \vdots & \iddots & \vdots \\ 0 & \cdots & 0 & \cdots & 0 & -b_{i1} & \cdots & -b_{ii} & \cdots & -b_{in} \\ \vdots & \iddots & \vdots & \ddots & \vdots & \vdots & \iddots & \vdots & \ddots & \vdots \\ 0 & \cdots & 0 & \cdots & 0 & -b_{n1} & \cdots & -b_{ni} & \cdots & -b_{nn} \\ \hline b_{11} & \cdots & b_{1i} & \cdots & b_{1n} & 0 & \cdots & 0 & \cdots & 0 \\ \vdots & \ddots & \vdots & \iddots & \vdots & \vdots & \ddots & \vdots & \iddots & \vdots \\ 0 & \cdots & 2 & \cdots & 0 & 0 & \cdots & 0 & \cdots & 0 \\ \vdots & \iddots & \vdots & \ddots & \vdots & \vdots & \iddots & \vdots & \ddots & \vdots \\ b_{n1} & \cdots & b_{ni} & \cdots & b_{nn} & 0 & \cdots & 0 & \cdots & 0 \end{array}\right] \quad (29)$$

Step 2) Run PCIPA to solve the voltage subproblem, and compute the complementary gap^v for voltage subproblem variables. If $gap^v/gap^a > \xi$, repeat solving this subproblem until $gap^v/gap^a \leq \xi$; otherwise, go to step 3.

Step 3) Update all variables.

Step 4) $i = i + 1$, check convergence of the subproblems. If the PCIPA barrier parameter μ^k is greater than ε_μ, go to step 1.

END DO

At steps 1 and 2, thresholds gap^a/gap^v and gap^v/gap^a are used to control the number of iterations to solve the active and voltage subproblems, respectively. This feature can help the robustness of the approach

Starting Point: A strictly feasible starting point is not mandatory for most IPA described. However, the primal and dual slack variables $(\underline{z}, \overline{z}, \underline{\omega}, \overline{\omega})$ must be strictly positive [17], [21]. IPA performs better if some initialization heuristics are used for defining a proper starting point [18]. The heuristics implemented are

- to estimate the primal variables x^0 as given in the base case, or as a flat start using the middle point between the upper and lower limits for the bounded variables;
- the primal slack variable can be chosen arbitrarily, so that $\omega^0 = \overline{h} - \underline{h}$;
- the Lagrange multipliers λ^0 can be simply set to zero and z^0 can be set to one.

Stopping Criteria: The PCIPA iterations are considered terminated whenever

$$\mu^k \leq \varepsilon_\mu$$
$$\|\Delta x\|_\infty \leq \varepsilon_x$$
$$\left\|g(x^k)\right\|_\infty \leq \varepsilon_x$$

are satisfied, where $\varepsilon_\mu = 10^{-8}$ and $\varepsilon_x = 10^{-4}$ are typical values and $\xi = 100$. If criteria $\|\Delta x\|_\infty \leq \varepsilon_x$ and $\|\Delta g(x^k)\|_\infty \leq \varepsilon_x$ are satisfied, then primal feasibility, scaled dual feasibility, and complimentarily conditions are all satisfied, that means iteration k is a KKT point of accuracy ε_x [18]. When numerical problems prevent verifying this condition, the algorithm stops as soon as the feasibility of the equality constraints is achieved along with very small fractional change in the objective value and negligible changes in the variables [17].

V. Numerical Results

This section presents some numerical results obtained with the implementation of PCIPA. The algorithm is tested on six different networks. All routines are written in MATLAB and run on a Pentium IV 2.8GHz with 516 Mb RAM. Table I shows the dimensions and summary of the test problems. The same minimization problem has been solved by three OPF codes including the rectangular **ECI_OPF**, decoupled ECI_OPF (**D_ECI_OPF**) of this research, and the traditional polar OPF (**NR_OPF**). Note that the LU decomposition was used in ECI_OPF and D_ECI_OPF, and the NR_OPF is based

TABLE I
Test Problem Statistics

Problem (BUS)	Size of Index Sets |N|	|G|	|B|	ECI_OPF Variables	ECI_OPF Constraints	NR_OPF Variables	NR_OPF Constraints
9	9	3	9	24	66	23	66
14	14	5	20	38	116	37	116
30	30	6	41	72	226	71	226
57	57	7	80	128	416	127	416
118	118	54	186	344	1060	343	1060
300	300	69	411	738	2298	737	2298

\|N\|: number of buses, \|G\|: number of generators, \|B\|: number of branches.

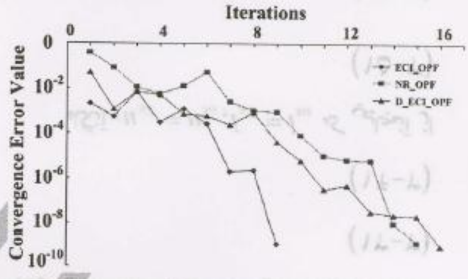

Fig. 3. Convergence error for 30-bus system.

on MATPOWER using quadratic programming technique with a Quasi-Newton approximation for the Hessian matrix [22]. MATPOWER provides a good MatlabTM Power System Simulation Package, and many studies have been successfully published [23], [24]. Note that NR_OPF has a different number of control variables, since NR_OPF has no swing theta variable.

All systems are IEEE standard systems derived from actual networks. The voltage limits are set as $\pm 5\%$ off-nominal for load buses and $\pm 10\%$ off-nominal for generator buses. The generator active/reactive power and the branch flow limits are set for each case.

Convergence Test: The convergence test used for the example is the IEEE 30-bus system. Fig. 3 shows the convergent errors for each of the three methods, with the stopping criteria set to 10^{-8}. It can be seen that ECI_OPF converges nicely, and it proves that IPA is indeed a better algorithm than NR [11]. NR_OPF and D_ECI_OPF need more iterations than ECI_OPF.

The values of objective functions for each iteration are shown in Fig. 4. The objective functions of the three OPF are around 775.39 $/MWh. The complementary gap is a very important measure to judge the optimality of solutions, and its changes reflect the characteristic of the algorithm. Fig. 5 shows how the gap and gap^* reduce with iterations for ECI_OPF. A good algorithm should decrease the complementary gap to zero monotonically and rapidly.

Performance Test: Table II shows the performance of all three methods. To assess the relative performance of the two proposed methods, each of the six systems was dispatched and started from two different starting points with and without heuristic rules. In all cases, the three algorithms performed well, with the number of iterations insensitive to the dimension of the problems. When converged, these methods always reached the same

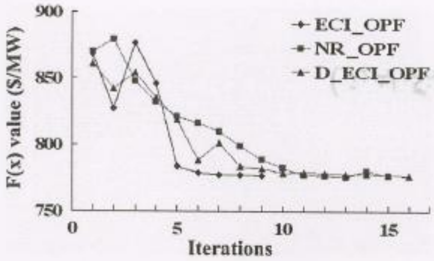

Fig. 4. Objection function value for 30-bus system.

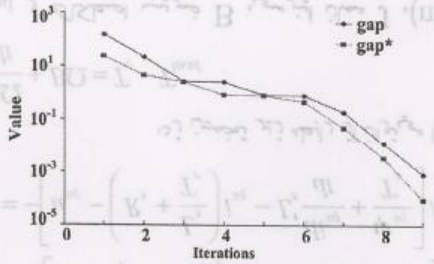

Fig. 5. ECI_OPF *gap* and *gap** value for 30-bus system.

TABLE II
ITERATIONS AND CPU TIMES OF NLP

Problem (BUS)	ECI_OPF (type1/type2)		D_ECI_OPF (type1/type2)		NR_OPF	
	Iterations	time (s)	Iterations	time (s)	Iterations	time (s)
9	8/8	0.08/0.08	15/15	0.07/0.07	14	0.58
14	8/7	0.18/0.16	16/15	0.10/0.09	15	1.17
30	9/7	0.86/0.67	16/15	0.71/0.58	15	4.88
57	10/8	1.97/1.64	19/17	1.71/1.52	17	14.47
118	12/11	6.39/5.95	21/19	5.79/5.17	19	55.06
300	16/14	40.8/38.23	24/22	33.2/30.74	22	362.25

type 1: without heuristic rules for starting point.
type 2: with heuristic rules for starting point.

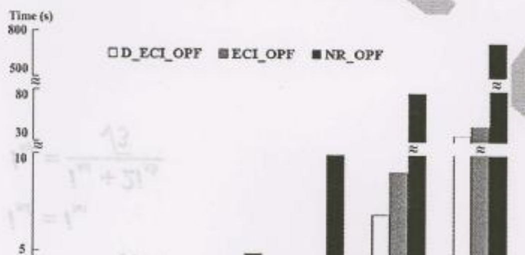

Fig. 6. CPU time comparison for type 2.

solution. In Table II and Fig. 6, we can observe that D_ECI_OPF is the best performer and NR_OPF takes more time to converge.

TABLE III
RESULTS OF DIFFERENT COORDINATION OPF WITH PCIPA

Task \ Method	D_ECI_OPF	ECI_OPF	P_OPF
Iterations	16	9	12
CPU time	0.71	0.86	2.20
Nonzero elements	1437	2598	4026

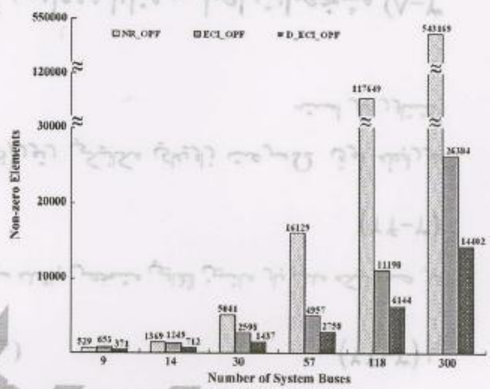

Fig. 7. Nonzero elements under different data structures.

A PCIPA-based polar coordinators OPF (P_OPF) published in [7] is also used for comparison, with the equality constraints of ECI_OPF and D_ECI_OPF replaced by the traditional Newton–Raphson power flow model as in [7]. Table III shows the performance and storage requirement for the IEEE 30-bus system, where no rules were taken for the starting points. All the OPF converge to the same solution, but D_ECI_OPF and ECI_OPF are better performers with less iterations and CPU time, and the nonzero elements of the proposed Hessian matrices are much less than that of the polar OPF.

Storage Test: Besides Table III, Fig. 7 also shows the number of nonzero Hessian elements for the test systems under the three structures. It is obvious that the elements of Hessian matrix in the D_ECI_OPF are much less than that of ECI_OPF and NR_OPF. It can be seen from (20) that ECI Hessian has a slightly bigger structure than NR Hessian. Using the ECI method is disadvantageous for smaller systems, such as the 9- or 14-bus systems. As the system grows, ECI method will outperform NR greatly since ECI matrix is sparse and contains mostly zeros, including both the Hessian and Jacobian matrices. For a daily operating large power network, ECI_OPF will have more advantages.

Robustness Test: Two cases are shown for the 30-bus system, which is known to be a relatively weaker system for testing.

A. Heavy Load Test

Fig. 8 is a heavy load test at bus 30. The load is adjusted by multiplying a factor W_1 that ranges from 0 to 2.1. When W_1 is 1.8, voltage sag occurs (0.94869 p.u.) at bus 30, and OPF needs more iterations to converge. Increasing W_1, the system further

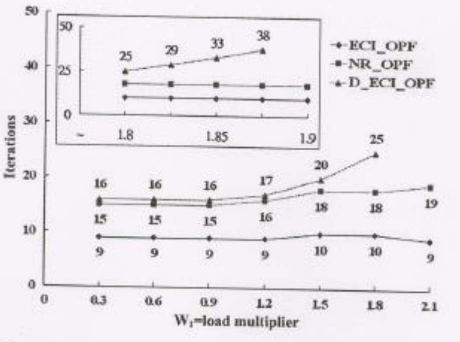

Fig. 8. Heavy load test at bus 30.

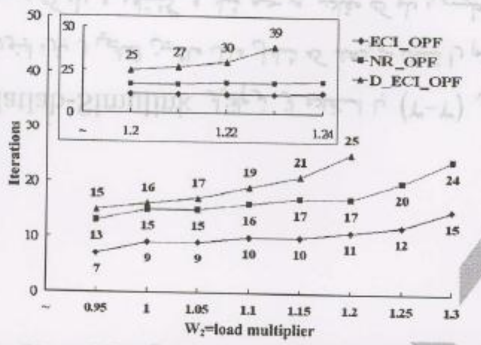

Fig. 9. Heavy load test for 30-bus system.

weakened, D_ECI_OPF can sustain a $W_1 > 1.8$, and ECI_OPF is the most robust.

The system worsens by adjusting a factor W_2 for all loads at the same time, as shown in Fig. 9. The factor W_2 changed from 0.95 to 1.3. When W_2 is 1.2, overload occurs at line 15–23, and all methods need more iterations to converge. As situations get worse, the network will have more and more violations and all OPFs are becoming unstable. It can be seen that the full ECI_OPF is the most robust of all, and D_ECI_OPF is strong enough to sustain a $W_2 > 1.2$. The tow full coupled OPF converge up to $W_2 = 1.3$ with more iterations.

B. R/X Ratio Test

Fig. 10 is an R/X ratio test for the three OPF methods. The R/X ratio is adjusted by multiplying a factor K that ranges from 0.5 to 6.0. Full coupled OPF is insensitive to the R/X ratio, and D_ECI_OPF converges up to $K > 4.15$, which is robust enough for most high voltage networks.

Starting Point Test: Since PCIPA is sensitive to the starting points, different settings were used to evaluate the impacts. All variables of starting points including primal, Lagrange multipliers, primal slack, and dual slack variables were all adjusted by multiplying a factor S for ECI_OPF and D_ECI_OPF. From Table IV, it can be seen that with S in the feasible range $0.67 \sim 3.35$ for ECI_OPF and $0.87 \sim 1.86$ for D_ECI_OPF, the two methods converge to the same solution without using heuristic rules. When the starting point is infeasible and set too far off

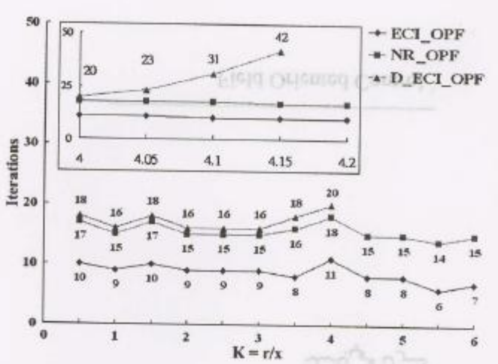

Fig. 10. R/X ratio test.

TABLE IV
RESULTS OF DIFFERENT STARTING POINT BY MULTIPLYING A FACTOR S

S	ECI OPF		S	D ECI OPF	
	Iterations	Cost [\$/h]		Iterations	Cost [\$/h]
0.6	19	778.51	0.8	21	780.28
0.7	8	775.39	0.9	15	775.39
1.0	9	775.39	1.0	16	775.39
3.3	10	775.39	1.8	18	775.39
3.4	11	775.48	1.9	20	776.24

the bounded limits (lower/upper than 0.66/3.36 for ECI_OPF, and lower/upper than 0.86/1.87 for D_ECI_OPF), PCIPA may or may not converge or converge prematurely to a different solution [18] as discussed in "the stopping criteria" in Section IV.

VI. CONCLUSIONS

In this paper, a new OPF framework has been presented. The algorithm uses the ECI-based formulation in the Cartesian coordinates and PCIPA. Extensive simulations on IEEE standard systems from 9 to 300 buses have verified that the proposed method is effective for power systems. Main properties of this approach are that

- the ECI model leads to a simple methodology if rectangular coordinates are adopted;
- a straightforward approach to deal with the PV bus is also proposed;
- ECI uses IPA with predictor-corrector mechanism which can effectively solve a modified OPF problem for minimum cost;
- ECI needs much lower storage for networks;
- ECI is accurate, robust, and very fast;
- a decoupled form D_ECI_OPF exists which can outperform the coupled methods, is accurate, robust, efficient, and needs lowest storage;
- full ECI_OPF can be used for extreme environments.

REFERENCES

[1] J. Carpentiers, "Contribution a. 'l'etude du dispatching economique," *Bull. Soc. Francaise Elect.*, vol. 3, pp. 431–447, 1962.
[2] M. Huneault and F. D. Galiana, "A survey of the optimal power flow literature," *IEEE Trans. Power Syst.*, vol. 6, no. 2, pp. 762–770, May 1991.

[3] G. Verbic and C. A. Canizares, "Probabilistic optimal power flow in electricity markets based on a two-point estimate method," *IEEE Trans. Power Syst.*, vol. 21, no. 4, pp. 1883–1893, Nov. 2006.
[4] A. J. Wood and B. F. Wollenberg, *Power Generation Operation and Control*. New York: Wiley, 1996.
[5] N. Karmarkar, "A new polynomial-time algorithm for linear programming," *Combinatorica*, vol. 4, pp. 373–395, May 1984.
[6] X. P. Zhang, S. G. Petoussis, and K. R. Godfrey, "Nonlinear interior-point optimal power flow method based on a current mismatch formulation," *Proc. Inst. Elect. Eng., Gen., Transm., Distrib.*, vol. 152, no. 6, pp. 795–805, Nov. 2005.
[7] Y. C. Wu, A. S. Debs, and R. E. Marsten, "A direct nonlinear predictor-corrector primal-dual interior point algorithm for optimal power flows," *IEEE Trans. Power Syst.*, vol. 9, no. 2, pp. 876–883, May 1994.
[8] R. A. Jabr, "Primal-dual interior-point approach to compute the L_1 solution of the state estimation problem," *Proc. Inst. Elect. Eng., Gen., Transm., Distrib.*, vol. 152, no. 3, pp. 313–320, May 2005.
[9] Q. Wei, A. J. Flueck, and T. Feng, "A new parallel algorithm for security constrained optimal power flow with a nonlinear interior point method," in *Proc. IEEE 2005 Power Eng. Soc. General Meeting*, Jun. 12–16, 2005, pp. 447–453.
[10] W. Yan, F. Liu, C. Y. Chung, and K. P. Wong, "A hybrid genetic algorithm-interior point method for optimal reactive power flow," *IEEE Trans. Power Syst.*, vol. 21, no. 3, pp. 1163–1169, Aug. 2006.
[11] H. Wei, H. Sasaki, and R. Yokoyama, "An interior point nonlinear programming for optimal power flow problems with a novel data structure," *IEEE Trans. Power Syst.*, vol. 13, no. 3, pp. 870–877, Aug. 1998.
[12] S. Mehrotra, "On the implementation of a primal-dual interior-point method," *SIAM J. Optim.*, pp. 575–601, Feb. 1992.
[13] W. F. Tinney, A Presentation to the Workshop in Engineering Mathematics and Computer Sciences, EPRI publication EAR/EL-7/07, pp. 1–15, Aug. 1991.
[14] W. M. Lin, Y. S. Su, H. C. Chin, and J. H. Teng, "Three-phase unbalanced distribution power flow solutions with minimum data preparation," *IEEE Trans. Power Syst.*, vol. 14, no. 3, pp. 1179–1183, Aug. 1999.
[15] W. M. Lin, T. S. Zhan, and M. T. Tsay, "Multiple-frequency three-phase load flow for harmonic analysis," *IEEE Trans. Power Syst.*, vol. 19, no. 2, pp. 897–904, May 2004.
[16] W. Rosehart and J. A. Aguado, "Alternative optimal power flow formulations," presented at the 14th Power System Computation Conf. (PSCC' 2002), Session 41, Jun. 24–28, 2002, paper 4, pp. 1–5, unpublished.
[17] G. L. Torres and V. H. Quintana, "An interior-point method for nonlinear optimal power flow using voltage rectangular coordinates," *IEEE Trans. Power Syst.*, vol. 13, no. 4, pp. 1211–1218, Nov. 1998.
[18] Y. C. Wu and A. S. Debs, "Initialization, decoupling, hot start, and warm start in direct nonlinear interior point algorithm for optimal power flows," *Proc. Inst. Elect. Eng., Gen., Transm., Distrib.*, vol. 148, no. 1, pp. 67–75, Jan. 2001.
[19] W. M. Lin and S. J. Chen, "Bid-based dynamic economic dispatch with and efficient interior point algorithm," *Int. J. EPES*, vol. 24, pp. 51–57, Apr. 2002.
[20] T. Xiaojiao, Z. Yongping, and F. F. Wu, "A decoupled Semismooth Newton method for optimal power flow," in *Proc. IEEE 2006 Power Eng. Soc. General Meeting*, Jun. 18–22, 2006, pp. 1–6.
[21] X. Yan and V. H. Quintana, "An efficient predictor-corrector interior point algorithm for security-constrained economic dispatch," *IEEE Trans. Power Syst.*, vol. 12, no. 2, pp. 1178–1183, May 1997.
[22] R. D. Zimmerman and D. Gan, MATPOWER-A Matlab Power System Simulation Package, Power Systems Engineering Research Center, Dec. 1997.
[23] D. Gan, D. Chattopadhyay, and X. Luo, "An improved method for optimal operation under stability constraints," in *Proc. 2003 IEEE Power Eng. Soc. Transmission and Distribution Conf. Expo.*, Sep. 7–12, 2003, vol. 2, pp. 683–688.
[24] D. Gan, R. J. Thomas, and R. D. Zimmerman, "Stability-constrained optimal power flow," *IEEE Trans. Power Syst.*, vol. 15, no. 2, pp. 535–540, May 2000.

Whei-Min Lin (M'87) was born on October 3, 1954. He received the B.S. degree in electrical engineering from the Natio[illegible]ao-Tung University, Hsinchu, Taiwan, R.O.C., [illegible] M.S. degree in electrical engineering from the University of Connecticut, Storrs, and the Ph.D. degree in electrical engineering from the University of Texas, Austin, in 1985. **AUTHOR: DO YOU WANT TO INCLUDE YEARS FOR FIRST 2 DEGREES?**

He worked at Chung-Hwa Institute for Economic Research, Taipei Taiwan, as a visiting researcher after his graduation. He joined Control Data Corporation, Minneapolis, MN, in 1986, and worked with Control Data Asia, Taipei, Taiwan, in 1989. He has been with National Sun Yat-Sen University, Kaohsiung, Taiwan, since 1991. His interests are GIS, distribution system, SCADA, and automatic control system.

Dr. Lin is a member of Tau Beta Pi.

Cong-Hui Huang was born on May 28, 1979. He received the B.S. degree in electrical engineering from the National Taiwan University of Science and Technology, Taipei, Taiwan, R.O.C., in 2001 and the M.S. degree in electrical engineering from the National Sun Yat-Sen University, Kaohsiung, Taiwan, in 2003, where he is currently pursuing the Ph.D. degree.

His research interests include power system operation, power system security, and power deregulation.

Tung-Sheng Zhan was born on November 9, 1975. He received the B.S. degree in electrical engineering from the National Yunlin University of Science and Technology, Yunlin, Taiwan, R.O.C., in 1997 and the M.S. degree in electrical engineering and Ph.D. degree from the National Sun Yan-Sen University, Kaohsiung, Taiwan, in 1999 and 2005, respectively.

He has been with Kao-Yuan University of Technology, Lu-Chu Hsiang, Kaohsiung, Taiwan, since 2000. His research interests are power system analysis, power deregulation, electricity markets, and AI optimal application.